



Article

Designing Potential Donor Materials Based on DRCN5T with Halogen Substitutions: A DFT/TDDFT Study

Yunjie Xiang^{1,2,*}, Jie Zhang^{1,2} and Shaohui Zheng^{1,2,*}

¹ School of Materials and Energy, Southwest University, Chongqing 400715, China; zjz123123@swu.edu.cn

² Chongqing Key Laboratory for Advanced Materials and Technologies of Clean Energies, Southwest University, Chongqing 400715, China

* Correspondence: hao1986kx88@swu.edu.cn (Y.X.); shaohuizheng@swu.edu.cn (S.Z.)

Abstract: Experimental researchers have found that the organic solar cell (OSC) based on DRCN5T (an oligothiophene) possesses excellent power conversion efficiency (PCE) of 10.1%. However, to date, there have been few studies about halogenation of DRCN5T, and its effects on photovoltaic properties of halogenated DRCN5T are still not clear. In the present work, we first perform benchmark calculations and effectively reproduce experimental results. Then, eight halogenated DRCN5T molecules are designed and investigated theoretically by using density functional theory (DFT) and time-dependent DFT. The dipole moments, frontier molecular orbital energies, absorption spectra, exciton binding energy (E_b), singlet–triplet energy gap (ΔE_{ST}), and electrostatic potential (ESP) of these molecules, and the estimated open circuit voltages (V_{OC} s) of the OSCs with PC₇₁BM as acceptor are presented. We find that (1) generally, halogen substitutions would increase V_{OC} ; (2) E_b rises with more fluorine substitutions, but for Cl and Br substitutions, E_b increases firstly and then drops; (3) ΔE_{ST} keeps increasing with more halogen substitutions; (4) except for Br substitutions, the averaged ESP arises along with more halogen substitutions; (5) the absorption strength of UV–Vis spectra of DRCN5T2F, DRCN5T4F, DRCN5T6F, and DRCN5T2Cl in the visible region is enhanced with respect to DRCN5T. Based on these results, overall, DRCN5T2Cl, DRCN5T4F, and DRCN5T6F may be promising donors.

Keywords: DFT; small organic solar cell; oligothiophenes; halogen substitutions; photovoltaic properties



Citation: Xiang, Y.; Zhang, J.; Zheng, S. Designing Potential Donor Materials Based on DRCN5T with Halogen Substitutions: A DFT/TDDFT Study. *Int. J. Mol. Sci.* **2021**, *22*, 13498. <https://doi.org/10.3390/ijms222413498>

Academic Editor: Mihai V. Putz

Received: 21 October 2021

Accepted: 14 December 2021

Published: 16 December 2021

Publisher's Note: MDPI stays neutral with regard to jurisdictional claims in published maps and institutional affiliations.



Copyright: © 2021 by the authors. Licensee MDPI, Basel, Switzerland. This article is an open access article distributed under the terms and conditions of the Creative Commons Attribution (CC BY) license (<https://creativecommons.org/licenses/by/4.0/>).

1. Introduction

Compared to polymer donors, small molecule donors possess several advantages such as easy purification, well-defined structures, and negligible batch-to-batch inconsistency. Oligothiophenes, as organic semiconductor materials, have been widely used in organic photovoltaics (OPVs) because they have excellent charge transport properties, tunable optical/electrochemical properties, high polarizability and high stability, relatively simple synthesis, and easy access [1–5]. Researchers have fabricated different OSCs based on oligothiophenes, and the PCEs of these OSCs are in the range of 1.49–10.1% [4–7]. Specifically, Chen and his co-workers have synthesized DRCN7T, a linear A-D-A (A: acceptor; D: donor) type of molecule with septithiophenes as a skeleton and 2-(1,1-dicyanomethylene) rhodanine as two end groups, and the organic solar cell (OSC) based on this synthesis has power conversion efficiency (PCE) of 9.3% [6]; later they reported a series of A-D-A molecules with different lengths of skeleton and the same end groups, namely DRCN n T ($n = 4\sim 9$), and they found that the conjugation length and spatial symmetry greatly affect molecular packing, phase separation, molecular orbital energy levels, and charge carrier mobility [7]. The most striking finding is that the OSC with DRCN5T (Figure 1) as a donor and PC₇₁BM as a acceptor achieves the PCE of 10.1%.

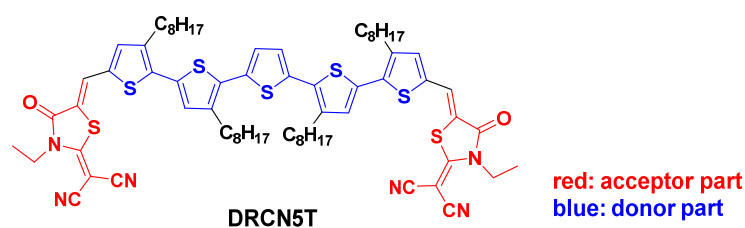


Figure 1. Molecular structure of DRCN5T.

Halogenation of organic molecules has been proved to be capable of improving opto-electronic performances: firstly it can increase the open circuit voltage (V_{OC}), which should be attributed to the deeper highest occupied molecular orbital (HOMO) energy level [8–13]; secondly, halogenations may improve the morphology of the active layer [14]. Peng's group [15] tuned the energetic structure of two polymers (PvBDT-F and PvBDT-Cl) via halogenation, and suitable absorption ranges and frontier molecular orbital energy levels were obtained when pairing with high performance NFA molecule Y6-T. The OSC with chlorinated PvBDT-Cl showed higher photovoltaic performances (PCE = 8.23%) than that with fluorinated PvBDT-F. Lu's group [16] chlorinated the original BTR donor molecule, which possessed strong intermolecular interaction, low-lying molecular energy levels, and a strong stacking tendency of edge-on orientation. Because of the different molecular packing orientations and different liquid crystalline properties between donor and acceptor, an appropriate morphology was achieved in the BTR-Cl:Y6 system, leading to a high PCE of 13.6% for all-small-molecule OSCs. Frequently, fluorine (F) and chlorine (Cl) atoms are introduced in donors to adjust the electronic structure and intermolecular interactions to obtain more efficient donors. So far, there are few studies about halogenation of DRCNnT. Beaujuge's group [17] reported a bulk-heterojunction solar cell with V_{OC} over 1.10 V with di-fluorinated DRCN5T as a donor and PC₇₁BM as an acceptor. Lu's group [18] studied the isomeric effect of fluorine substitution on the performance of solar cells based on di-fluorinated DRCN5T (donor):IDIC4F (acceptor). However, until now, studies about fluorination of DRCN5T have lacked clarity and theoretical insights. Furthermore, there is no research about chlorine and bromine substitutions of DRCN5T. In brief, a systematic study of halogenation of DRCN5T is needed to consider the potential of DRCN5T.

Therefore, in this work, we have systematically modelled new molecules DRCN5T4F, DRCN5T6F, DRCN5T2Cl, DRCN5T4Cl, DRCN5T6Cl, DRCN5T2Br, DRCN5T4Br, and DRCN5T6Br, as shown in Figure 2. These molecules are rationally and systematically designed with different numbers of halogen atoms. For instance, DRCN5T2Cl and DRCN5T2Br have exactly the same substituted positions as DRCN5T2F. Similarly, the halogen substitutions of DRCN5T4X and DRCN5T6X are highly possible and should be synthesized in experiments. By substitutions with halogen atoms, we have modified the chemical structure, charge distribution, and planarity of these molecules. We plan to investigate the effects on the photovoltaic performance of these molecules. We utilize density functional theory (DFT) and time-dependent DFT (TDDFT) to study how different halogen substitutions influence opto-electronical properties such as dipole moments, frontier molecular orbitals (FMOs), energy gap, UV-Vis spectra, and V_{OC} s (with PC₇₁BM as acceptor), exciton binding energy, ΔE_{ST} , and ESP of these molecules. The theoretical studies about predicting the opto-electronic properties of newly designed small photovoltaic molecules have been shown to be quite reliable [19].

In particular, the dipole moment of a small molecule is important. With a proper dipole moment, relatively good charge separation and stacking morphology can be obtained to achieve high PCE [18]. Researchers have investigated the triplet behavior of DRCN5T [20], but they have not studied the effect of ΔE_{ST} (energy of S_1 minus energy of T_1) on DRCN5T and its halogenated derivatives to further understand the importance of triplet state. ΔE_{ST} is a crucial parameter for developing organic photovoltaic materials. Small ΔE_{ST} generally decreases the charge recombination in exciton dissociation and voltage loss. So here it is important to investigate the above properties.

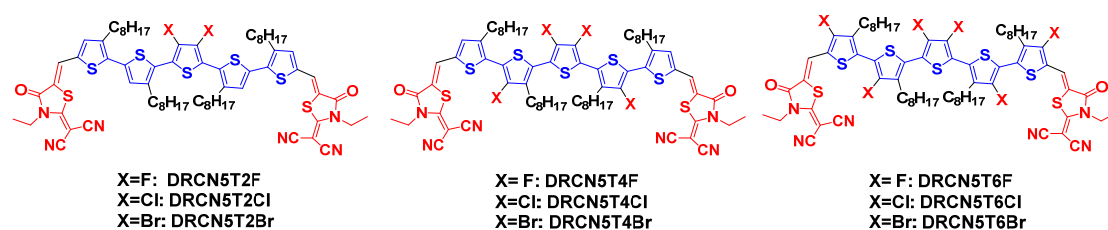


Figure 2. Molecular structures of DRCN5T2X, DRCN5T4X, and DRCN5T6X (X = F, Cl, and Br).

The purposes of this work are twofold:

- (1) To investigate the effects of different halogen substitutions and the extent of halogenation on the photovoltaic properties of DRCN5T.
- (2) To find new promising donors (if possible) based on DRCN5T.

2. Results and Discussion

2.1. Benchmark Calculations

We make use of CAM-B3LYP, tuned ω B97X, and B3LYP density functionals [21] with 6–31+G(d) to run TDDFT calculations of DRCN5T and DRCN5T2F molecules. Figure 3 shows the results of absorption spectra of DRCN5T and DRCN5T2F, based on the TDDFT outputs of CAM-B3LYP, B3LYP, and tuned ω B97X density functionals in chloroform (same as the experiment). The simulated absorption spectra of DRCN5T and DRCN5T2F with CAM-B3LYP functional are the closest to the experimental ones in the visible region. The wavelength of experimental absorption peaks of DRCN5T and DRCN5T2F is located at 531 nm and 500 nm, respectively [7,18]. As shown in Table S1, the wavelength of the absorption peaks of DRCN5T and DRCN5T2F obtained with CAM-B3LYP functional is located at 589 and 569 nm, respectively. However, for the results of ω B97X and B3LYP, the wavelengths of absorption peaks of both molecules are 688/663 nm and 766/731 nm, respectively. Obviously, CAM-B3LYP is superior to the other two density functionals. Regarding these data in Table 1, we conclude that the CAM-B3LYP is suitable for excited state calculations.

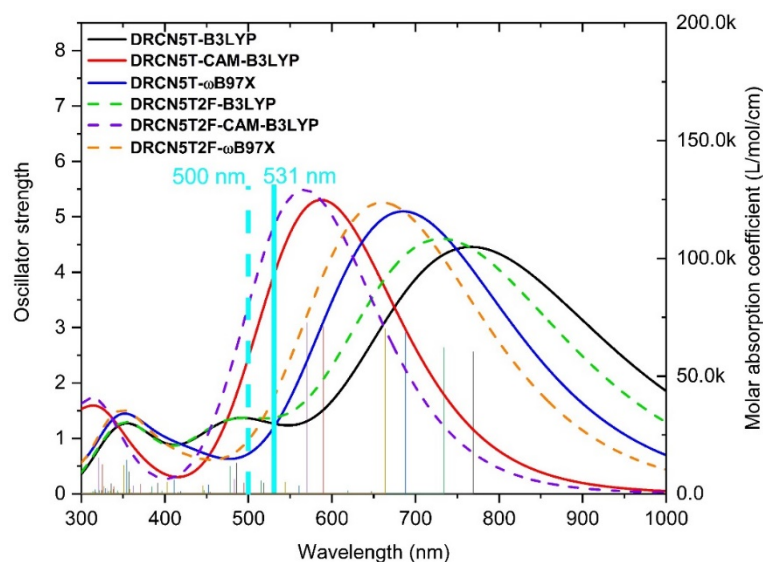


Figure 3. Simulated UV-Vis spectra of DRCN5T and DRCN5T2F with FWHM of 0.6667 eV based on different functionals with 6–31+G(d) basis set (black curve: B3LYP for DRCN5T; red: CAM-B3LYP for DRCN5T; blue: ω B97X for DRCN5T; green: B3LYP for DRCN5T2F; purple: CAM-B3LYP for DRCN5T2F; yellow: ω B97X for DRCN5T2F; line in light blue: experimental λ_{\max} of DRCN5T; dashed line in light blue: experimental λ_{\max} of DRCN5T2F) in chloroform.

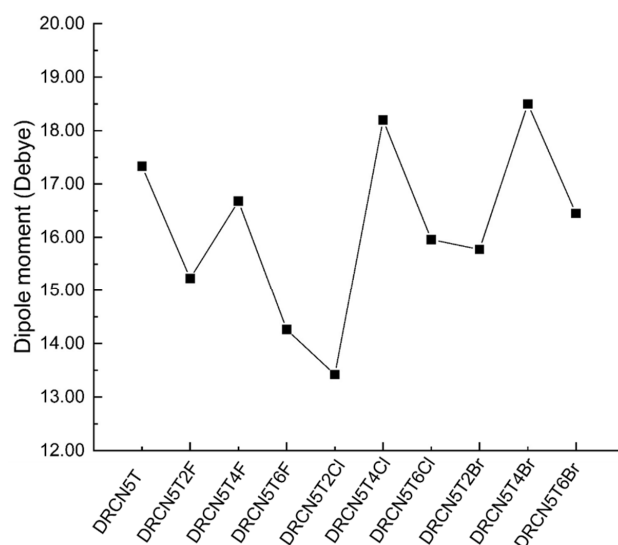
Table 1. The experimental and calculated absorption peaks in the visible region and corresponding energy of DRCN5T and DRCN5T2F.

| DRCN5T | Experiment | | | | CAM-B3LYP | ω B97X | B3LYP |
|-------------|-----------------------|------|------|------|-----------|---------------|-------|
| | λ_{\max} (nm) | 531 | 589 | 688 | 766 | | |
| energy (eV) | 2.34 | 2.11 | 1.80 | 1.62 | | | |
| DRCN5T2F | Experiment | | | | CAM-B3LYP | ω B97X | B3LYP |
| | λ_{\max} (nm) | 500 | 569 | 663 | 731 | | |
| energy (eV) | 2.48 | 2.18 | 1.87 | 1.70 | | | |

Based on the comparisons between experiments and the calculated data, we thus choose CAM-B3LYP as the most accurate functional to calculate DRCN5T, DRCN5T2F, and eight new designed halogenated derivatives.

2.2. Dipole Moments of the Halogenated Molecules

Dipole moments are related to the molecular packing and charge separation [22]. When the dipole moment increases, the charge separation is enhanced. However, if the dipole moment is too large, the molecules will aggregate unnecessarily, so the value of the dipole moment should be appropriate. As shown in Figure 4, DRCN5T, DRCN5T2F, DRCN5T4F, DRCN5T6F, DRCN5T2Cl, DRCN5T4Cl, DRCN5T6Cl, DRCN5T2Br, DRCN5T4Br, and DRCN5T6Br possess the dipole moments of 17.33, 15.23, 16.68, 14.26, 13.42, 18.20, 15.96, 15.78, 18.50, and 16.45 Debye, respectively. DRCN5T has been proved to exhibit effective molecular packing between molecules [7]. However, it can be further improved. One good example is DRCN5T2F, synthesized by Lu and co-workers [18], which has a dipole moment of 15.23 Debye, slightly smaller than that of DRCN5T (17.33 Debye). Consequently, it does not aggregate as much as DRCN5T in experiments (Root-mean-square surface roughness is 3.15 nm for DRCN5T:IDIC-4F, only 2.43 nm for DRCN5T2F:IDIC-4F by AFM), enhancing the fill factor and short circuit current [18]. The PCE of the OSC with IDIC-4F as an acceptor and DRCN5T2F as donor was increased to 9.36% (the PCE of the OSC based on DRCN5T/IDIC-4F is 8.02%) [18]. As shown in Figure 4, DRCN5T2F, DRCN5T4F, DRCN5T6F, DRCN5T2Cl, DRCN5T6Cl, DRCN5T2Br, and DRCN5T6Br have slightly smaller dipole moments (15.23, 16.68, 14.26, 13.42, 15.96, 15.78, and 16.45 Debye, respectively) than that of DRCN5T (17.33 Debye), which may benefit a higher PCE [23,24].

**Figure 4.** The calculated dipole moments of DRCN5T, DRCN5T2F, DRCN5T4F, DRCN5T6F, DRCN5T2Cl, DRCN5T4Cl, DRCN5T6Cl, DRCN5T2Br, DRCN5T4Br, and DRCN5T6Br gained with CAM-B3LYP/6-31+G(d) in film.

In Figure 4, DRCN5T2F (chemical structure is shown in Figure 2) has a smaller dipole moment than that of DRCN5T because two electron-withdrawing F atoms (two F at up positions on thiophene ring) shorten the distance between positive and negative charge centers of DRCN5T2F. From DRCN5T2F to DRCN5T4F to DRCN5T6F, the dipole moment first increases and then drops because four electron-withdrawing F atoms (two at up and two at down positions on thiophene rings) make the distance between the opposite charge centers longer, and six electron-withdrawing F atoms (four at up and two at down positions on thiophene rings) shorten the distance again. For Cl- and Br-substituted molecules, their dipole moments have the same trends. DRCN5T2Cl has the smaller dipole moment than that of DRCN5T2F owing to the stronger electron-withdrawing effects of 2Cl relative to 2F, which makes the distance between opposite charge centers shorter. DRCN5T2Br possesses the biggest dipole moment among DRCN5T2F, DRCN5T2Cl, and DRCN5T2Br on account of the weakest electron-withdrawing effects of 2Br.

2.3. LUMO/HOMO Energy and Energy Gap of the Halogenated Molecules

DRCN5T is substituted by different numbers of halogens to generate new molecules: DRCN5T4F, DRCN5T6F, DRCN5T2Cl, DRCN5T4Cl, DRCN5T6Cl, DRCN5T2Br, DRCN5T4Br and DRCN5T6Br, respectively. Figure 2 shows the chemical structures of the eight new halogenated molecules. We utilize CAM-B3LYP density functional to calculate LUMO/HOMO energy and energy gap of the eight molecules. The results are displayed in Figure 5. The experimental HOMO/LUMO of DRCN5T and DRCN5T2F are -5.22 eV / -3.41 eV [7] and -5.34 eV / -3.59 eV, respectively [18]. Comparing the calculated data with the experimental values further confirms the accuracy of our chosen methods. The HOMO energy of the eight new molecules becomes lower after halogenation and the energy gaps become bigger than that of DRCN5T because of the electron-withdrawing ability of halogens. Additionally, the value of HOMO of DRCN5T4Cl, DRCN5T6Cl, DRCN5T2Br, DRCN5T4Br, and DRCN5T6Br drops a lot, which results in a significant increase in their V_{OC} s. The energy gaps of DRCN5T4Cl, DRCN5T6Cl, DRCN5T2Br, DRCN5T4Br, and DRCN5T6Br are higher than the others (DRCN5T2F, DRCN5T4F, DRCN5T6F, DRCN5T2Cl) by at least 0.3 eV, which may be mainly attributed to their non-planarity [25] (see Figure S1). In Figure S1, the selected dihedral angles ψ_1 and ψ_2 of DRCN5T4Cl, DRCN5T6Cl, DRCN5T2Br, DRCN5T4Br, and DRCN5T6Br are between 77° and 90° , indicating their strong non-planarity. While DRCN5T2F, DRCN5T4F, DRCN5T6F, and DRCN5T2Cl have planar structures. The radius of Cl and Br atoms are larger than that of F atoms, which causes the stronger non-planarity of DRCN5T after being substituted by them.

2.4. V_{OC} of the OSC with Halogenated Molecules as Donors

Open circuit voltage (V_{OC}) is one of important factors that influence the PCE of OSCs. We use the empirical formula reported by Scharber et al. to calculate V_{OC} s of OSCs based on these new molecules with PC₇₁BM as acceptor [26]. The calculated LUMO/HOMO energy and energy gap of PC₇₁BM by CAM-B3LYP is -3.01 eV, -5.78 eV, and 2.77 eV, respectively. Table 2 shows the calculated V_{OC} values of the OSCs with these new molecules as donors (utilizing Equation (10)). Due to the introduction of electron-withdrawing halogen atoms, the HOMO of the substituted molecule decreases, leading to the increase in V_{OC} (Equation (10)). The V_{OC} rises with the increasing number of the substituted halogen because of the stronger electron-withdrawing ability of halogens (DRCN5T2F < DRCN5T4F < DRCN5T6F, DRCN5T2Cl < DRCN5T4Cl < DRCN5T6Cl, DRCN5T2Br < DRCN5T4Br < DRCN5T6Br). Additionally, the V_{OC} becomes larger after chlorine and bromine substitutions. These results indicate that the type of the substituted halogen atoms has a great influence on V_{OC} .

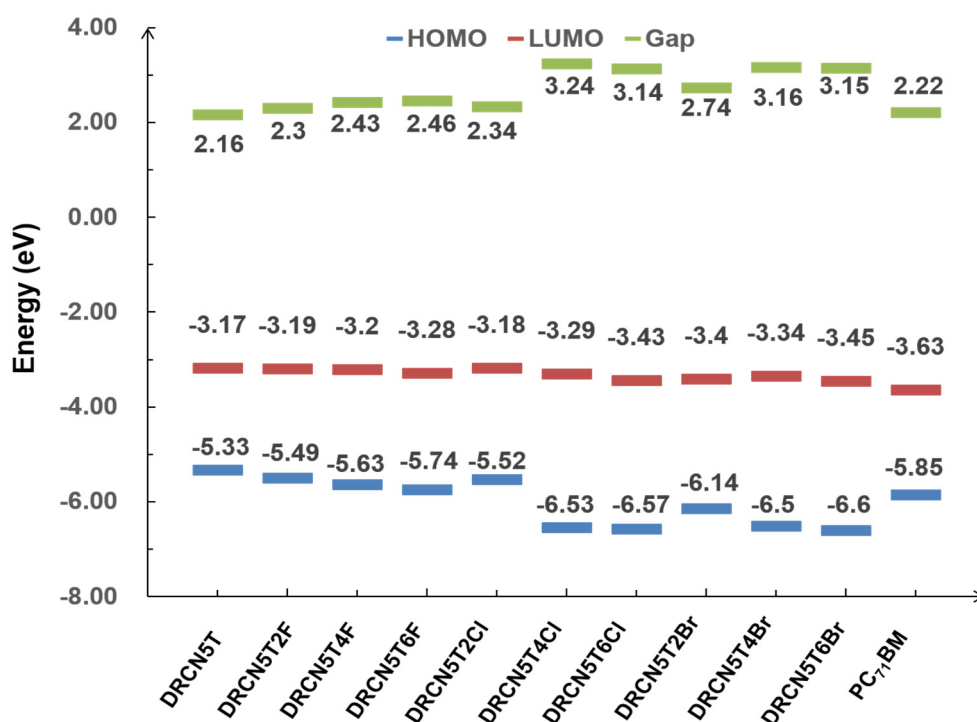


Figure 5. Calculated LUMO, HOMO and gap of DRCN5T, DRCN5T2F, DRCN5T4F, DRCN5T6F, DRCN5T2Cl, DRCN5T4Cl, DRCN5T6Cl, DRCN5T2Br, DRCN5T4Br, and DRCN5T6Br by using CAM-B3LYP/6–31+ G(d) in dichloromethane.

Table 2. The predicted V_{OC} of OSCs with DRCN5T and its derivatives as donor and PC₇₁BM as acceptor via Equation (10). EA/IP correction denotes the absolute value of $EA_{D, film} - EA_{D, vacuum}$ or $IP_{D, film} - IP_{D, vacuum}$, respectively. Unit: V for V_{OC} ; eV for energy. Cor: Corrected; Exp: Experimental. In order to be consistent with the experimental value, we make corrections to all calculated V_{OC} s, i.e., $Cor V_{OC} = V_{OC} - 1.33$ V, in which 1.33 V is the V_{OC} deviation between experiment and calculation of DRCN5T/PC₇₁BM OSC.

| | DRCN-5T | DRCN-5T2F | DRCN-5T4F | DRCN-5T6F | DRCN-5T2Cl | DRCN-5T4Cl | DRCN-5T6Cl | DRCN-5T2Br | DRCN-5T4Br | DRCN-5T6Br |
|---------------|----------|-----------|-----------|-----------|------------|------------|------------|------------|------------|------------|
| HOMO | -6.43 | -6.57 | -6.74 | -6.90 | -7.22 | -7.65 | -7.78 | -7.04 | -7.73 | -7.81 |
| LUMO | -2.49 | -2.53 | -2.57 | -2.69 | -2.34 | -2.24 | -2.36 | -2.25 | -2.21 | -2.34 |
| IP correction | 0.80 | 0.79 | 0.80 | 0.83 | 0.79 | 0.81 | 0.85 | 0.79 | 0.79 | 0.87 |
| EA correction | 0.50 | 0.49 | 0.47 | 0.44 | 0.72 | 0.50 | 0.49 | 0.72 | 0.52 | 0.51 |
| V_{OC} | 2.32 | 2.47 | 2.63 | 2.76 | 3.12 | 3.53 | 3.62 | 2.94 | 3.62 | 3.63 |
| Cor V_{OC} | 0.99 | 1.14 | 1.30 | 1.43 | 1.79 | 2.20 | 2.29 | 1.61 | 2.29 | 2.30 |
| Exp V_{OC} | 0.99 [7] | 1.12 [17] | N/A | N/A | N/A | N/A | N/A | N/A | N/A | N/A |

2.5. Inner Reorganization Energy

Inner reorganization energy (λ_i) is the energy required for the change in geometric structure in the process of charge transport. The smaller the inner reorganization energy, the smaller the energy loss, and maybe the higher carrier mobility [27]. However, the carrier mobility is related to not only λ_i , but also the external reorganization energy, the electronic coupling, and charge transfer distance [28]. The inner reorganization energy of DRCN5T, DRCN5T2F, DRCN5T4F, DRCN5T6F, DRCN5T2Cl, DRCN5T4Cl, DRCN5T6Cl, DRCN5T2Br, DRCN5T4Br, and DRCN5T6Br is calculated by using CAM-B3LYP/6–31+G(d) via Equation (12), as displayed in Figure 6. The inner reorganization energy of DRCN5T and these nine halogenated molecules is 0.30, 0.31, 0.30, 0.29, 0.82, 1.12, 0.77, 0.76, 1.22, 1.17 eV. DRCN5T2F, DRCN5T4F, and DRCN5T6F have almost the same level of inner reorganization energy as DRCN5T; DRCN5T6F has the smallest one

(0.29 eV). The chlorine and bromine substituted DRCN5T derivatives have a much higher inner reorganization energy than that of DRCN5T and fluorine-substituted derivatives.

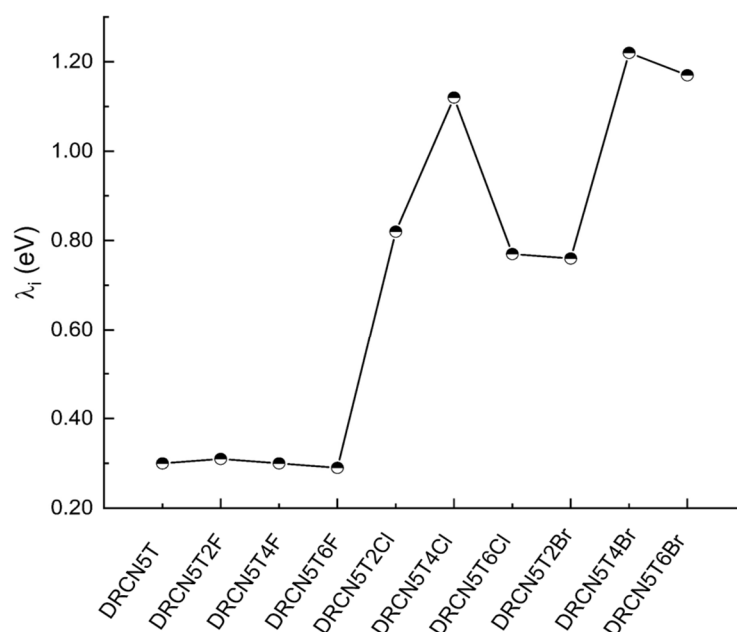


Figure 6. Calculated inner reorganization energies (eV) of DRCN5T, DRCN5T2F, DRCN5T4F, DRCN5T6F, DRCN5T2Cl, DRCN5T4Cl, DRCN5T6Cl, DRCN5T2Br, DRCN5T4Br, and DRCN5T6Br by using CAM-B3LYP/6–31+G(d) in film.

2.6. Exciton Binding Energy of the Nine Halogenated Molecules

Exciton binding energy is the energy used to separate excitons into hole and electron in organic solar cells. Small exciton binding energy should benefit J_{SC} , charge separation, and PCE [29]. We present the calculated exciton binding energy of DRCN5T2F, DRCN5T4F, DRCN5T6F, DRCN5T2Cl, DRCN5T4Cl, DRCN5T6Cl, DRCN5T2Br, DRCN5T4Br, and DRCN5T6Br gained with CAM-B3LYP/6–31+G(d) in film. As shown in Figure 7 and Table S2, exciton binding energy is calculated by Equation (13). The exciton binding energy of DRCN5T and these nine molecules is 0.52, 0.58, 0.64, 0.67, 0.45, 0.87, 0.86, 0.56, 1.23 and 0.94 eV, respectively. The exciton binding energy of fluorine-substituted molecules increases with more fluorine substitutions. For Cl- and Br-substituted molecules, with the increase in the number of substitutions, the exciton binding energy first increases and then decreases. For DRCN5T2Cl, the fundamental gap (IP–EA) is 3.17 eV, and E_{opt} is 2.72 eV, so it obtains the lowest exciton binding energy of 0.45 eV; for DRCN5T4Br, the fundamental gap (IP–EA) increases to 4.45 eV, and its E_{opt} is 3.22 eV, therefore the exciton binding energy is the largest with the value of 1.23 eV (Table S2). DRCN5T2Cl possesses the smallest value of exciton binding energy, followed by DRCN5T, DRCN5T2Br, DRCN5T2F, DRCN5T4F, and then DRCN5T6F. The value of IP minus EA decreases, and it is closer to the optical gap, making the exciton binding energy of DRCN5T2Cl the smallest. Based on these results, DRCN5T2Cl molecule may be a potential donor material due to its small exciton binding energy.

2.7. Singlet–Triplet Energy Gap of the Nine Halogenated Molecules

Singlet–triplet energy gap (ΔE_{ST}) represents the energy difference between the lowest triplet (T_1) and singlet (S_1) excited states. Additionally, it is equal to the sum of ΔE_{CT} and ΔE_{BET} [30]. ΔE_{CT} means the drive force of charge-transfer (CT) state, and a small ΔE_{CT} can reduce the voltage loss to increase open-circuit voltage. ΔE_{BET} represents the difference between CT and T_1 energies. By back electron transfer (BET), the triplet CT exciton can relax to the triplet state (T_1) and charges can recombine. The reduced ΔE_{BET} can improve

the speed of T_1 to thermalize back into CT state and reduce the recombination of triplet charge transport excitons. As such, low ΔE_{ST} can effectively reduce the voltage loss in the exciton dissociation [31] and charge recombination through triplet state [20,30]. The results of ΔE_{ST} of the nine halogenated molecules calculated by Equations (16)–(18) were shown in Figure 8 and Table S3. The ΔE_{ST} generally increases with more halogen substitutions on account of the stronger electron-withdrawing ability of halogens (DRCN5T2F < DRCN5T4F < DRCN5T6F, DRCN5T2Cl < DRCN5T4Cl < DRCN5T6Cl, DRCN5T2Br < DRCN5T4Br < DRCN5T6Br). Additionally, the values of ΔE_{ST} for Cl- and Br-substituted molecules are higher than those of F-substituted molecules. The halogenated molecules DRCN5T2F, DRCN5T4F, DRCN5T6F, DRCN5T2Cl, and DRCN5T2Br have a similar level of ΔE_{ST} to DRCN5T (small ΔE_{ST} of 1.19 eV). Based on these results, they may be promising photovoltaic materials.

2.8. ESP of the Nine New Molecules

It can be seen from Figure 9 that with more F and Cl substitutions, the electrostatic potential (ESP) rises. Additionally, as the ESP difference between the donor and the acceptor becomes bigger, the interaction between them increases [32]. The enhanced intermolecular interaction will increase the charge-transfer (CT) state ratio, but at the same time will cause a larger E_{loss} , which is not conducive to photoelectric conversion efficiency [32]. Therefore, it is necessary to find a suitable number of F and Cl substitutions [33]. The tetrafluoro substitution is moderate with the averaged ESP of 224 meV. Dichloro and tetrachloro substitutions have almost the same averaged ESP, and their values are moderate. However, the ESP of Br-substituted molecules does not rise along with the increase in the number of substituted Br atoms. The averaged ESP (221 meV) of DRCN5T2Br is moderate. On the other hand, the averaged ESPs of DRCN5T2F, DRCN5T4F, DRCN5T6F, DRCN5T2Cl, DRCN5T4Cl, and DRCN5T2Br are higher than that of DRCN5T (195 meV), indicating that they are potential donors. Based on all the above results, the tetrafluoro substitution donor (DRCN5T4F) is the ideal donor among the difluoro, tetrafluoro, and hexafluoro substitution donors.

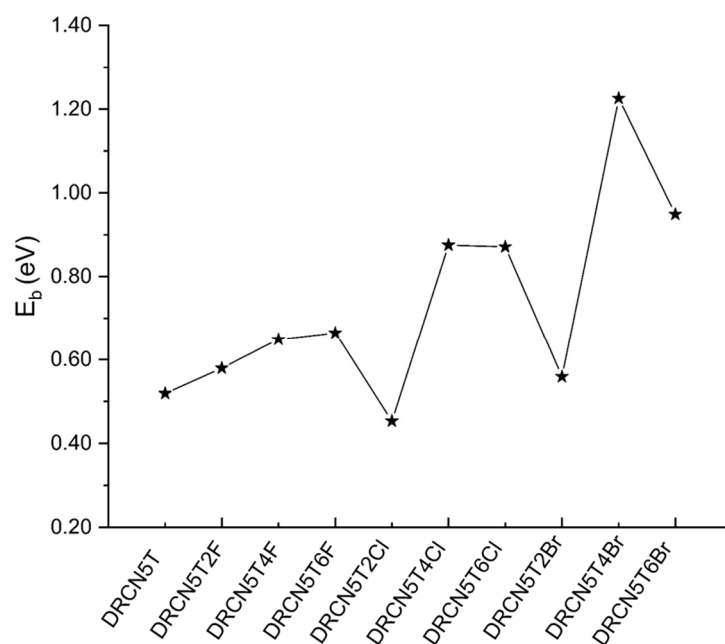


Figure 7. The calculated exciton binding energy of DRCN5T, DRCN5T2F, DRCN5T4F, DRCN5T6F, DRCN5T2Cl, DRCN5T4Cl, DRCN5T6Cl, DRCN5T2Br, DRCN5T4Br, and DRCN5T6Br with CAM-B3LYP/6-31+G(d) in film ($\epsilon = 3.0$).

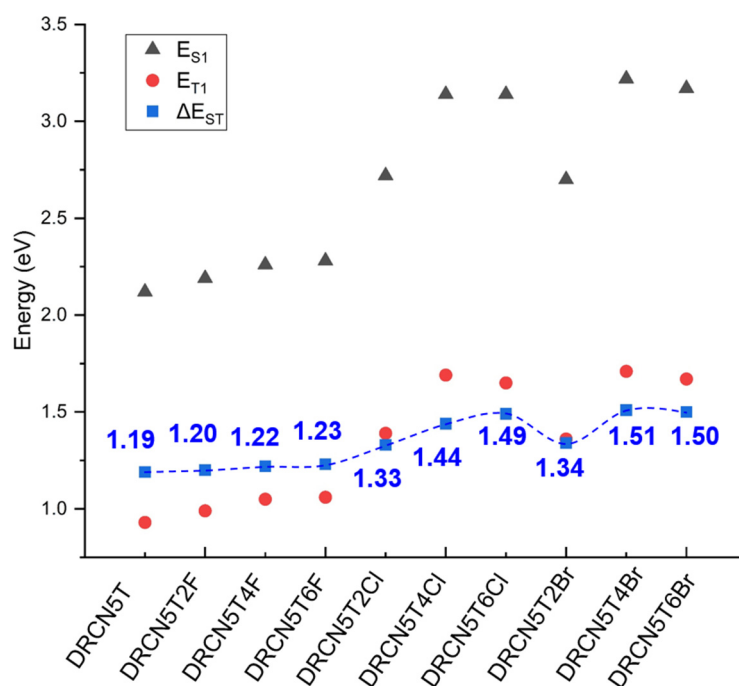


Figure 8. The lowest singlet (E_{S1}), triplet excited energy (E_{T1}) and singlet–triplet energy gap (ΔE_{ST}) of DRCN5T, DRCN5T2F, DRCN5T4F, DRCN5T6F, DRCN5T2Cl, DRCN5T4Cl, DRCN5T6Cl, DRCN5T2Br, DRCN5T4Br, and DRCN5T6Br with CAM-B3LYP/6–31+G(d) in film ($\epsilon = 3.0$).

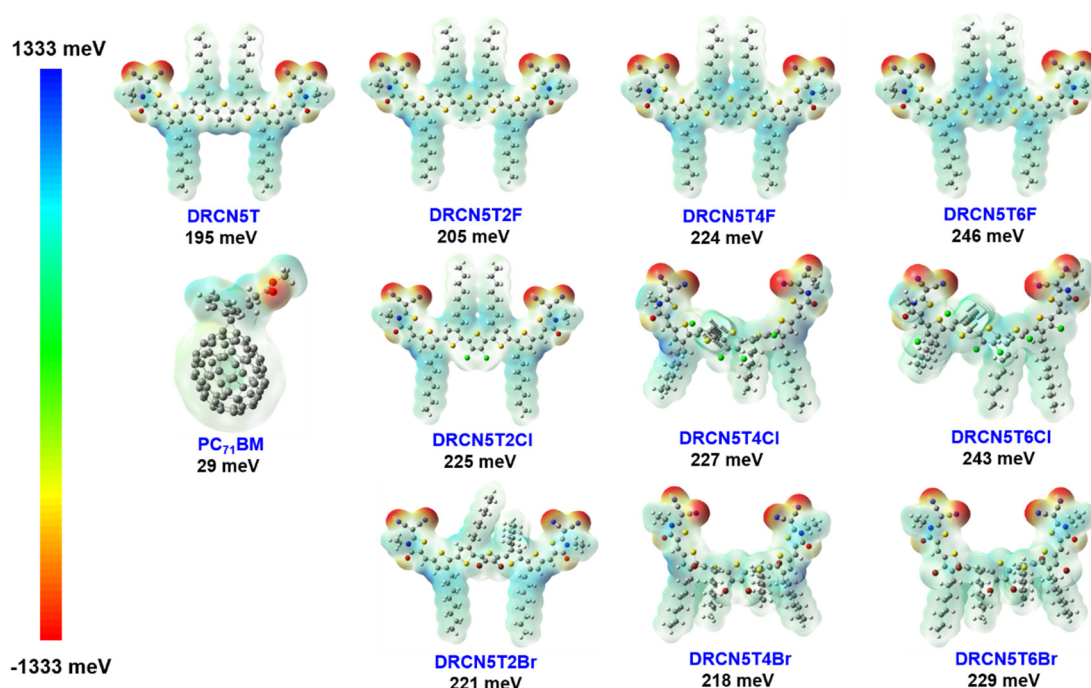


Figure 9. Averaged ESP of DRCN5T, DRCN5T2F, DRCN5T4F, DRCN5T6F, DRCN5T2Cl, DRCN5T4Cl, DRCN5T6Cl, DRCN5T2Br, DRCN5T4Br, DRCN5T6Br, and PC₇₁BM calculated on B3LYP/6–31G(d) level.

2.9. UV–Vis Spectra of the Designed New Molecules

As shown in Figure 10, UV–Vis spectra of DRCN5T4F, DRCN5T6F, DRCN5T2Cl, DRCN5T4Cl, DRCN5T6Cl, DRCN5T2Br, DRCN5T4Br, and DRCN5T6Br in chloroform with CAM-B3LYP functional are calculated. Table S4 shows the results of simulated excited states. For DRCN5T2F, DRCN5T4F, DRCN5T6F, DRCN5T2Cl, DRCN5T4Cl, DRCN5T6Cl,

DRCN5T2Br, DRCN5T4Br and DRCN5T6Br, the maximum absorption peak is at 569 nm, 551 nm, 547 nm, 561 nm, 393 nm, 397 nm, 459 nm, 384 nm and 391 nm, respectively. The wavelength of these absorption peaks is blue-shifted compared to that of DRCN5T (Figures 10 and 11) owing to the electron-withdrawing ability of halogens. As can be seen, the wavelength of DRCN5T4Cl, DRCN5T6Cl, DRCN5T2Br, DRCN5T4Br, and DRCN5T6Br blue-shifts a lot among these new molecules because of their larger fundamental energy gap (Figures 10 and 11). Table S5 shows the calculated main absorption wavelength, main transition, and percentage of the transition. As can be seen from Table S5, for DRCN5T2F, DRCN5T4F, DRCN5T6F, and DRCN5T2Cl with planar structure, the main transition is HOMO to LMUO with percentage about 77%. Additionally, for non-planar DRCN5T4Cl, DRCN5T6Cl, DRCN5T2Br, DRCN5T4Br, and DRCN5T6Br, HOMO-1 to LUMO+1, HOMO to LUMO, HOMO-1 to LUMO and HOMO to LUMO+1 are the main transitions.

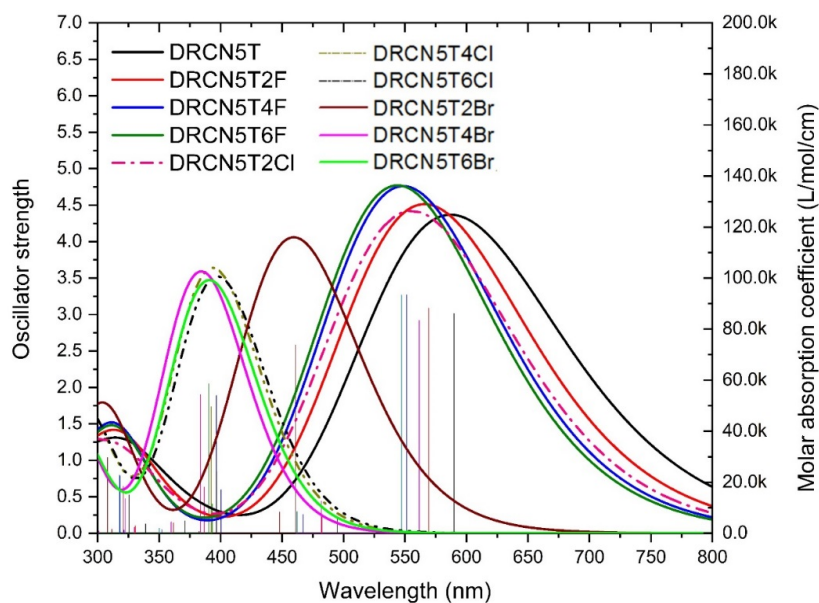


Figure 10. Calculated UV-Vis spectra of eight designed molecules obtained with CAM-B3LYP/6-31+ G(d) in PCM model.

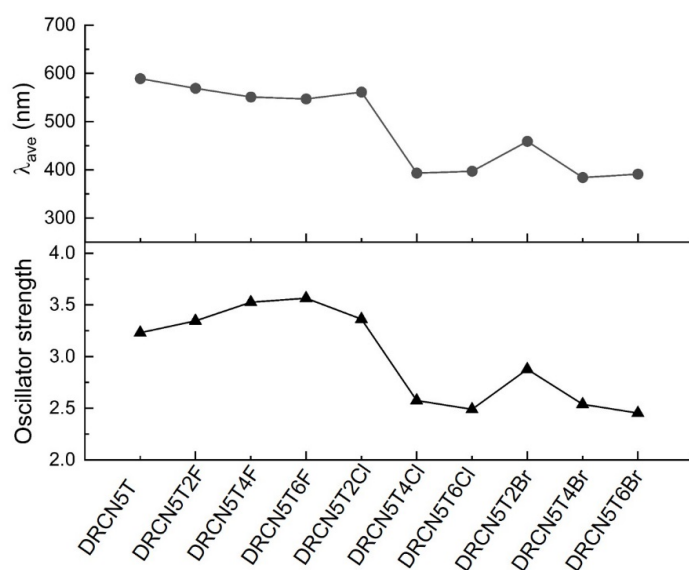


Figure 11. The averaged wavelength of absorption peaks and the total oscillator strength of the halogenated molecules.

The oscillator strength of DRCN5T4Cl, DRCN5T6Cl, DRCN5T4Br, and DRCN5T6Br decreases significantly compared with that of DRCN5T (Figure 11), which might be caused by their reduced planarity [25]. The oscillator strength of DRCN5T2F, DRCN5T4F, DRCN5T6F, and DRCN5T2Cl increases in contrast to that of DRCN5T. Based on these results, we may conclude that DRCN5T2F, DRCN5T4F, DRCN5T6F, and DRCN5T2Cl may be the better candidates for solar cells.

3. Methods

All molecular structures were built with GaussView version 5.0 [34]. Additionally, all calculations were calculated by using Gaussian09 Rev E.01 software package [35]. To take into account environment effects, we used integral equation formalism variant polarizable continuum models (IEF-PCM) [36,37]. In order to compare with experiments, the energy of LUMO (lowest unoccupied molecular orbital), HOMO (highest occupied molecular orbital), and gap was computed in dichloromethane with a dielectric constant (ϵ) of 8.93, and the calculation of excited states for simulation of absorption spectra was carried out in chloroform with ϵ of 4.7113. As for thin film, ϵ was set to 3.0 since the values of dielectric constants of organic photovoltaic materials are around 3.0 [19,38]. DRCN5T, DRCN5TnF, DRCN5TnCl, and DRCN5TnBr ($n = 2, 4, 6$) molecules were optimized with the combination of B3LYP [38] hybrid density functional and 6–31G(d) basis set, which has been demonstrated as reliable for geometric optimization of organic molecules [39,40]. 6–31+G(d) basis set was selected for the rest of the calculations, and the added diffusion function is more accurate for weak interactions and excited states systems [41,42].

Firstly, we run benchmark calculations to obtain a suitable density functional by comparing absorption spectra with the available experimental data. CAM-B3LYP [43], ω B97X [44], and B3LYP density functionals were chosen. Among them, ω B97X and CAM-B3LYP are long range corrected (LRC) density functionals, which are more accurate in principle because they partly cure the derivative discontinuity problem and self-interaction error of traditional density functionals.

In order to gain accurate HOMO/LUMO energy in solution, we calculated the energy of FMOs with the equations as follows [45]:

$$\epsilon'_H = \epsilon_H + [IP^{gas-phase} - IP^{PCM}] \quad (1)$$

$$\epsilon'_L = \epsilon_L + [EA^{gas-phase} - EA^{PCM}] \quad (2)$$

$$IP^{gas-phase} = E(N-1) - E(N) \quad (3)$$

$$EA^{gas-phase} = E(N) - E(N+1) \quad (4)$$

$$IP^{PCM} = E^{PCM}(N-1) - E^{PCM}(N) \quad (5)$$

$$EA^{PCM} = E^{PCM}(N) - E^{PCM}(N+1) \quad (6)$$

where ϵ_H / ϵ_L represents the HOMO/LUMO energy of neutral system in gas phase at the equilibrium geometry obtained within PCM, respectively; $\epsilon'_H / \epsilon'_L$ represents the corrected HOMO/LUMO energy in condensed phase, respectively; N denotes the neutral system; EA/IP means electron affinity/ionization potential, respectively.

The system-dependent parameter ω of LRC density functional ω B97X [46] was obtained by using the following equations [46]:

$$J^2(\omega) = J_N^2(\omega) + J_{N+1}^2(\omega) \quad (7)$$

$$J_N^2(\omega) = [\epsilon_{HOMO}^\omega(N) + E^\omega(N-1) - E^\omega(N)]^2 \quad (8)$$

$$J_{N+1}^2(\omega) = [\epsilon_{HOMO}^\omega(N+1) + E^\omega(N) - E^\omega(N+1)]^2 \quad (9)$$

where $E^\omega(N)$ is the energy of neutral system; $\varepsilon_{HOMO}^\omega(N)$ is the energy of HOMO of neutral system; $E^\omega(N+1)$ represents the energy of anion; $E^\omega(N-1)$ is the energy of cation. The optimized ω s are 0.08 Bohr^{-1} for both DRCN5T and DRCN5T2F.

We roughly predicted open circuit voltages of OSCs with PC₇₁BM as an acceptor by using the following empirical equation [26]:

$$V_{OC} = (1/e) \left(\left| E_{HOMO}^{Donor} \right| - \left| E_{LUMO}^{PCBM} \right| \right) - 0.3 \quad (10)$$

where e is the electron charge; E_{HOMO}^{Donor} means the energy of HOMO of donor; E_{LUMO}^{PCBM} denotes the energy of LUMO of acceptor PC₇₁BM.

Multiwfn 3.8 software package was selected to simulate the absorption spectrum with the output of 40 excited states [47]. Additionally, the full width at half maximum (FWHM) of absorption peak was default (0.6667 eV). For the wavelength of simulated absorption peaks, the following equation was used:

$$\lambda_{ave} = \frac{\sum \lambda_n \times f_n}{\sum f_n} \quad (11)$$

where λ_{ave} represents the wavelength of absorption peak; f_n denotes the oscillator strength of the n th excited state; λ_n is the wavelength of the n th excited state.

The following equation was used to calculate the inner reorganization energy [28,48]:

$$\lambda_{i,h} = \left[E^0(D^+) - E^0(D^0) \right] + \left[E^+(D^0) - E^+(D^+) \right] \quad (12)$$

where $\lambda_{i,h}$ is the inner reorganization energy; $E^0(D^+)$ is the total energy of neutral donor in the optimized geometry of cation; $E^0(D^0)$ represents the total energy of neutral donor in the optimized geometry of neutral molecule; $E^+(D^0)$ denotes energy of positive donor in the optimized geometry of neutral molecule; $E^+(D^+)$ is energy of positive donor in the optimized geometry of cation.

Exciton binding energy is a key factor in influencing charge transfer and separation. The following equations were used to calculate exciton binding energy with IEF-PCM [49,50]:

$$E_b = E_g^{fund} - E_g^{opt} \quad (13)$$

$$E_g^{fund} = E(N-1) + E(N+1) - 2E(N) \quad (14)$$

$$E_g^{opt} = E(N, Excited) - E(N) \quad (15)$$

where E_b is exciton binding energy; E_g^{opt} denotes the energy of optical gap; E_g^{fund} is the energy of fundamental gap; $N/N+1/N-1$ represents a neutral/anion/cation system, respectively.

The singlet–triplet energy gap (ΔE_{ST}) is an important parameter for organic photovoltaic materials and denotes the energy difference between the lowest singlet (S_1) and triplet (T_1) excited states [30]. ΔE_{ST} was calculated as follows [51].

$$\Delta E_{ST} = E_{S1} - E_{T1} = \Delta E_{CT} + \Delta E_{BET} \quad (16)$$

$$\Delta E_{CT} = E_{S1} - E_{CT} \quad (17)$$

$$\Delta E_{BET} = E_{CT} - E_{T1} \quad (18)$$

4. Conclusions

By using DFT and TDDFT calculations, we have studied the effects of halogen substitution on the physical and opto-electronic properties of these new molecules. From DRCN5T2F to DRCN5T4F to DRCN5T6F, the dipole moment first increases and then decreases. For Cl- and Br-substituted molecules, their dipole moments have the same

tendency as F-substituted molecules. Halogenated molecules with a slightly smaller dipole moment than that of DRCN5T possibly enhance fill factor and PCE of OSCs. The HOMO energy of DRCN5T4Cl, DRCN5T6Cl, DRCN5T2Br, DRCN5T4Br, and DRCN5T6Br greatly reduces due to their non-planarity, which leads to a significant increase in their V_{OCs} . The lowest inner reorganization energy of DRCN5T6F may indicate the smallest energy loss. The exciton binding energy (E_b) of fluorine-substituted molecules rises with more fluorine substitutions. For Cl- and Br-substituted molecules, with the increase in the number of substitutions, E_b increases at first and then reduces. DRCN5T2Cl exhibits the smallest value of E_b , indicating that it may be a potential donor material. DRCN5T2F, DRCN5T4F, DRCN5T6F, DRCN5T2Cl, and DRCN5T2Br have a similar ΔE_{ST} to DRCN5T, demonstrating that they may be promising photovoltaic materials. DRCN5T4F may be the ideal donor among the difluoro, tetrafluoro, and hexafluoro substitutions donors based on the moderate averaged ESP. Compared to DRCN5T, DRCN5T2F, DRCN5T4F, DRCN5T6F, and DRCN5T2Cl possess the enhanced oscillator strength of UV-Vis spectra. In summary, we may conclude that DRCN5T2Cl, DRCN5T4F, and DRCN5T6F have the potential to be good donors. Our work may provide a guideline for future halogenation modification of DRCN5T and lay the foundations for the development of oligothiophene-based donors.

Supplementary Materials: The following are available online at <https://www.mdpi.com/article/10.3390/ijms22413498/s1>.

Author Contributions: Investigation, Y.X. and J.Z.; Methodology, Y.X.; Supervision, Y.X. and S.Z.; Writing—original draft, Y.X.; Writing—review and editing, S.Z. All authors have read and agreed to the published version of the manuscript.

Funding: This research was funded by National Natural Science Foundation of China, grant number 21801211 and by Natural Science Foundation of Chongqing, China, grant number cstc2019jcyj-msxmX0137.

Institutional Review Board Statement: Not applicable.

Informed Consent Statement: Not applicable.

Data Availability Statement: Not applicable.

Acknowledgments: We greatly appreciate the financial support from National Natural Science Foundation of China (21801211) and Natural Science Foundation of Chongqing, China (cstc2019jcyj-msxmX0137). S. Z. greatly thanks the Natural Science Foundation of Chongqing, China (cstc2021jcyj-msxmX0964) for their financial support.

Conflicts of Interest: The authors declare no conflict of interest.

References

1. Liu, Y.S.; Zhou, J.Y.; Wan, X.J.; Chen, Y.S. Synthesis and Properties of Acceptor-Donor-Acceptor Molecules Based on Oligothiophenes with Tunable and Low Band Gap. *Tetrahedron* **2009**, *65*, 5209–5215. [[CrossRef](#)]
2. Liu, Y.S.; Wan, X.J.; Wang, F.; Zhou, J.Y.; Long, G.K.; Tian, J.G.; Chen, Y.S. High-Performance Solar Cells Using a Solution-Processed Small Molecule Containing Benzodithiophene Unit. *Adv. Mater.* **2011**, *23*, 5387–5391. [[CrossRef](#)]
3. Lin, Y.Z.; Li, Y.F.; Zhan, X.W. Small Molecule Semiconductors for High-Efficiency Organic Photovoltaics. *Chem. Soc. Rev.* **2012**, *41*, 4245–4272. [[CrossRef](#)]
4. Zhang, L.; Colella, N.S.; Cherniawski, B.P.; Mannsfeld, S.C.B.; Briseno, A.L. Oligothiophene Semiconductors: Synthesis, Characterization, and Applications for Organic Devices. *ACS Appl. Mater. Interfaces* **2014**, *6*, 5327–5343. [[CrossRef](#)]
5. Fitzner, R.; Mena-Osteritz, E.; Mishra, A.; Schulz, G.; Reinold, E.; Weil, M.; Körner, C.; Ziehlke, H.; Elschner, C.; Leo, K.; et al. Correlation of Pi-Conjugated Oligomer Structure with Film Morphology and Organic Solar Cell Performance. *J. Am. Chem. Soc.* **2012**, *134*, 11064–11067. [[CrossRef](#)] [[PubMed](#)]
6. Zhang, Q.; Kan, B.; Liu, F.; Long, G.; Wan, X.; Chen, X.; Zuo, Y.; Ni, W.; Zhang, H.; Li, M.; et al. Small-Molecule Solar Cells with Efficiency over 9%. *Nat. Photonics* **2015**, *9*, 35–41. [[CrossRef](#)]
7. Kan, B.; Li, M.; Zhang, Q.; Liu, F.; Wan, X.; Wang, Y.; Ni, W.; Long, G.; Yang, X.; Feng, H.; et al. A Series of Simple Oligomer-like Small Molecules Based on Oligothiophenes for Solution-Processed Solar Cells with High Efficiency. *J. Am. Chem. Soc.* **2015**, *137*, 3886–3893. [[CrossRef](#)]
8. Ye, L.; Zhang, S.Q.; Huo, L.J.; Zhang, M.J.; Hou, J.H. Molecular Design toward Highly Efficient Photovoltaic Polymers Based on Two-Dimensional Conjugated Benzodithiophene. *Acc. Chem. Res.* **2014**, *47*, 1595–1603. [[CrossRef](#)] [[PubMed](#)]

9. Li, W.; Albrecht, S.; Yang, L.; Roland, S.; Tumbleston, J.R.; McAfee, T.; Yan, L.; Kelly, M.A.; Ade, H.; Neher, D.; et al. Mobility-Controlled Performance of Thick Solar Cells Based on Fluorinated Copolymers. *J. Am. Chem. Soc.* **2014**, *136*, 15566–15576. [[CrossRef](#)] [[PubMed](#)]
10. Ni, W.; Wan, X.J.; Li, M.M.; Wang, Y.C.; Chen, Y.S. A-D-A Small Molecules for Solution-Processed Organic Photovoltaic Cells. *Chem. Commun.* **2015**, *51*, 4936–4950. [[CrossRef](#)]
11. Liu, P.; Zhang, K.; Liu, F.; Jin, Y.C.; Liu, S.J.; Russell, T.P.; Yip, H.L.; Huang, F.; Cao, Y. Effect of Fluorine Content in Thienothiophene-Benzodithiophene Copolymers on the Morphology and Performance of Polymer Solar Cells. *Chem. Mat.* **2014**, *26*, 3009–3017. [[CrossRef](#)]
12. Min, J.; Zhang, Z.-G.; Zhang, S.; Li, Y. Conjugated Side-Chain-Isolated D–A Copolymers Based on Benzo[1,2-*b*:4,5-*b'*]dithiophene-alt-dithienylbenzotriazole: Synthesis and Photovoltaic Properties. *Chem. Mat.* **2012**, *24*, 3247–3254. [[CrossRef](#)]
13. Liu, X.R.; Shen, W.; He, R.X.; Luo, Y.F.; Li, M. Strategy to Modulate the Electron-Rich Units in Donor-Acceptor Copolymers for Improvements of Organic Photovoltaics. *J. Phys. Chem. C* **2014**, *118*, 17266–17278. [[CrossRef](#)]
14. Peet, J.; Senatore, M.L.; Heeger, A.J.; Bazan, G.C. The Role of Processing in the Fabrication and Optimization of Plastic Solar Cells. *Adv. Mater.* **2009**, *21*, 1521–1527. [[CrossRef](#)]
15. Zhang, M.; Xu, X.; Yu, L.; Peng, Q. Efficient Wide-band-gap Copolymer Donors for Organic Solar Cells with Perpendicularly Placed Benzodithiophene Units. *J. Power Sources* **2021**, *499*, 229961. [[CrossRef](#)]
16. Chen, H.; Hu, D.; Yang, Q.; Gao, J.; Fu, J.; Yang, K.; He, H.; Chen, S.; Kan, Z.; Duan, T.; et al. All-Small-Molecule Organic Solar Cells with an Ordered Liquid Crystalline Donor. *Joule* **2019**, *3*, 3034–3047. [[CrossRef](#)]
17. Babics, M.; Duan, T.; Balawi, A.H.; Liang, R.; Cruciani, F.; Carja, I.; Gottlieb, D.; McCulloch, I.; Vandewal, K.; Laquai, F.; et al. Negligible Energy Loss During Charge Generation in Small-Molecule/Fullerene Bulk-Heterojunction Solar Cells Leads to Open-Circuit Voltage over 1.10 V. *ACS Appl. Energy Mater.* **2019**, *2*, 2717–2722. [[CrossRef](#)]
18. Duan, T.; Gao, J.; Babics, M.; Kan, Z.; Zhong, C.; Singh, R.; Yu, D.; Lee, J.; Xiao, Z.; Lu, S. Difluorinated Oligothiophenes for High-Efficiency All-Small-Molecule Organic Solar Cells: Positional Isomeric Effect of Fluorine Substitution on Performance Variations. *Sol. RRL* **2020**, *4*, 1900472. [[CrossRef](#)]
19. Qiu, W.; Zheng, S. Designing and Screening High-Performance Non-Fullerene Acceptors: A Theoretical Exploration of Modified Y6. *Sol. RRL* **2021**, *5*, 2100023. [[CrossRef](#)]
20. Marin-Beloqui, J.; Toolan, D.; Panjwani, N.; Limbu, S.; Kim, J.; Clarke, T.M. Triplet-Charge Annihilation in a Small Molecule Donor: Acceptor Blend as a Major Loss Mechanism in Organic Photovoltaics. *Adv. Energy Mater.* **2021**, *11*, 2100539. [[CrossRef](#)]
21. Li, G.; Zheng, S. A Computational Study of the Effects of Axial Halogen Substitutions of Boron Subphthalocyanines on their Electronic Spectra in Solution and in the Solid State. *Spectrochim Acta A* **2019**, *222*, 117180. [[CrossRef](#)] [[PubMed](#)]
22. Xu, B.; Yi, X.; Huang, T.; Zheng, Z.; Zhang, J.; Salehi, A.; Coropceanu, V.; Hoi Yi Ho, C.; Marder, S.R.; Toney, M.F.; et al. Donor Conjugated Polymers with Polar Side Chain Groups: The Role of Dielectric Constant and Energetic Disorder on Photovoltaic Performance. *Adv. Funct. Mater.* **2018**, *28*, 1803418. [[CrossRef](#)]
23. Sciuto, G.L.; Capizzi, G.; Salvatore, C.O.C.O.; Shikler, R. Geometric Shape Optimization of Organic Solar Cells for Efficiency Enhancement by Neural Networks. In *Advances on Mechanics, Design Engineering and Manufacturing*; Springer: Cham, Switzerland, 2017; pp. 789–796.
24. Capizzi, G.; Lo Sciuto, G.; Napoli, C.; Shikler, R.; Woźniak, M. Optimizing the Organic Solar Cell Manufacturing Process by Means of AFM Measurements and Neural Networks. *Energies* **2018**, *11*, 1221. [[CrossRef](#)]
25. Xu, X.; Zheng, S. Designing New Donor Materials Based on Functionalized DCCnT with Different Electron-Donating Groups: A Density Functional Theory (DFT) and Time Dependent Density Functional Theory (TDDFT)-Based Study. *Int. J. Quantum Chem.* **2019**, *120*, e26112. [[CrossRef](#)]
26. Scharber, M.C.; Wuhlbacher, D.; Koppe, M.; Denk, P.; Waldauf, C.; Heeger, A.J.; Brabec, C.L. Design Rules for Donors in Bulk-Heterojunction Solar Cells—Towards 10% Energy-Conversion Efficiency. *Adv. Mater.* **2006**, *18*, 789–794. [[CrossRef](#)]
27. Pablo-Pedro, R.; Lopez-Rios, H.; Mendoza-Cortes, J.; Kong, J.; Fomine, S.; Van Voorhis, T.; Dresselhaus, M. Exploring Low Internal Reorganization Energies for Silicene Nanoclusters. *Phys. Rev. Appl.* **2018**, *9*, 054012. [[CrossRef](#)]
28. Xu, C.; Xu, X.; Zheng, S. On the Relations between Backbone Thiophene Functionalization and Charge Carrier Mobility of A–D–A type Small Molecules. *New J. Chem.* **2020**, *44*, 15177–15185. [[CrossRef](#)]
29. Kraner, S.; Prampolini, G.; Cuniberti, G. Exciton Binding Energy in Molecular Triads. *J. Phys. Chem. C* **2017**, *121*, 17088–17095. [[CrossRef](#)]
30. Han, G.; Hu, T.; Yi, Y. Reducing the Singlet–Triplet Energy Gap by End-Group π – π Stacking Toward High-Efficiency Organic Photovoltaics. *Adv. Mater.* **2020**, *32*, 2000975. [[CrossRef](#)] [[PubMed](#)]
31. Benatto, L.; de Almeida Sousa, K.R.; Koehler, M. Driving Force for Exciton Dissociation in Organic Solar Cells: The Influence of Donor and Acceptor Relative Orientation. *J. Phys. Chem. C* **2020**, *124*, 13580–13591. [[CrossRef](#)]
32. Yao, H.; Cui, Y.; Qian, D.; Ponseca, C.S., Jr.; Honarfar, A.; Xu, Y.; Xin, J.; Chen, Z.; Hong, L.; Gao, B.; et al. 14.7% Efficiency Organic Photovoltaic Cells Enabled by Active Materials with a Large Electrostatic Potential Difference. *J. Am. Chem. Soc.* **2019**, *141*, 7743–7750. [[CrossRef](#)]
33. Xu, Y.; Yao, H.; Ma, L.; Hong, L.; Li, J.; Liao, Q.; Zu, Y.; Wang, J.; Gao, M.; Ye, L.; et al. Tuning the Hybridization of Local Exciton and Charge-Transfer States in Highly Efficient Organic Photovoltaic Cells. *Angew. Chem. Int. Ed.* **2020**, *59*, 9004–9010. [[CrossRef](#)]
34. Dennington, R.K.T.; Millam, J. *GaussView, Version 5*; Semichem Inc.: Shawnee Mission, KS, USA, 2009.

35. Frisch, M.J. *Gaussian 2009 Revision D.01*; Gaussian Inc.: Wallingford, CT, USA, 2009.
36. Jacobson, L.D.; Herbert, J.M. Polarization-Bound Quasi-Continuum States Are Responsible for the “Blue Tail” in the Optical Absorption Spectrum of the Aqueous Electron. *J. Am. Chem. Soc.* **2010**, *132*, 10000–10002. [[CrossRef](#)]
37. Zheng, S.; Geva, E.; Dunietz, B.D. Solvated Charge Transfer States of Functionalized Anthracene and Tetracyanoethylene Dimers: A Computational Study Based on a Range Separated Hybrid Functional and Charge Constrained Self-Consistent Field with Switching Gaussian Polarized Continuum Models. *J. Chem. Theory Comput.* **2013**, *9*, 1125–1131. [[CrossRef](#)]
38. Stephens, P.J.; Devlin, F.J.; Chabalowski, C.F.; Frisch, M.J. Ab-Initio Calculation of Vibrational Absorption and Circular-Dichroism Spectra Using Density-Functional Force-Fields. *J. Phys. Chem.* **1994**, *98*, 11623–11627. [[CrossRef](#)]
39. Hehre, W.J.; Ditchfield, R.; Pople, J.A. Self-Consistent Molecular-Orbital Methods XII. Further Extensions of Gaussian-Type Basis Sets for Use in Molecular-Orbital Studies of Organic-Molecules. *J. Chem. Phys.* **1972**, *56*, 2257–2261. [[CrossRef](#)]
40. Xiao, M.; Tian, Y.; Zheng, S. An Insight into the Relationship between Morphology and Open Circuit Voltage/Electronic Absorption Spectrum at Donor-Acceptor Interface in Boron Subphthalocyanine Chloride/C70 Solar Cell: A DFT/TDDFT Exploration. *Org. Electron.* **2018**, *59*, 279–287. [[CrossRef](#)]
41. Elsayed, S.A.; El-Gharabawy, H.M.; Butler, I.S.; Atlam, F.M. Novel Metal Complexes of 3-acetylcoumarin-2-hydrazinobenzothiazole Schiff Base: Design, Structural Characterizations, DNA Binding, DFT Calculations, Molecular Docking and Biological Studies. *Appl. Organomet. Chem.* **2020**, *34*, e5643. [[CrossRef](#)]
42. McCarthy, M.; Lee, K.L.K. Molecule Identification with Rotational Spectroscopy and Probabilistic Deep Learning. *J. Phys. Chem. A* **2020**, *124*, 3002–3017. [[CrossRef](#)]
43. Yanai, T.; Tew, D.P.; Handy, N.C. A New Hybrid Exchange–Correlation Functional Using the Coulomb-Attenuating Method (CAM-B3LYP). *Chem. Phys. Lett.* **2004**, *393*, 51–57. [[CrossRef](#)]
44. Chai, J.D.; Head-Gordon, M. Long-Range Corrected Hybrid Density Functionals with Damped Atom-Atom Dispersion Corrections. *Phys. Chem. Chem. Phys.* **2008**, *10*, 6615–6620. [[CrossRef](#)]
45. Phillips, H.; Zheng, Z.; Geva, E.; Dunietz, B.D. Orbital Gap Predictions for Rational Design of Organic Photovoltaic Materials. *Org. Electron.* **2014**, *15*, 1509–1520. [[CrossRef](#)]
46. Sun, H.T.; Zhong, C.; Sun, Z.R. Recent Advances in the Optimally “Tuned” Range-Separated Density Functional Theory. *Acta Phys. Chim. Sin.* **2016**, *32*, 2197–2208. [[CrossRef](#)]
47. Lu, T.; Chen, F. Multiwfn: A Multifunctional Wavefunction Analyzer. *J. Comput. Chem.* **2012**, *33*, 580–592. [[CrossRef](#)] [[PubMed](#)]
48. Nelsen, S.F.; Blackstock, S.C.; Kim, Y. Estimation of Inner Shell Marcus Terms for Amino Nitrogen Compounds by Molecular Orbital Calculations. *J. Am. Chem. Soc.* **1987**, *109*, 677–682. [[CrossRef](#)]
49. Lee, J.-C.; Chai, J.-D.; Lin, S.-T. Assessment of Density Functional Methods for Exciton Binding Energies and Related Optoelectronic Properties. *RSC Adv.* **2015**, *5*, 101370–101376. [[CrossRef](#)]
50. Chen, X.; Zheng, S. On the Study of Influence of Molecular Arrangements and Dipole Moment on Exciton Binding Energy in Solid State. *Int. J. Quantum Chem.* **2020**, *121*, e26511. [[CrossRef](#)]
51. Menke, S.M.; Sadhanala, A.; Nikolka, M.; Ran, N.A.; Ravva, M.K.; Abdel-Azeim, S.; Stern, H.L.; Wang, M.; Sirringhaus, H.; Thuc-Quyen, N.; et al. Limits for Recombination in a Low Energy Loss Organic Heterojunction. *ACS Nano* **2016**, *10*, 10736–10744. [[CrossRef](#)] [[PubMed](#)]